



NO reduction by CO over NiO_x/CeO₂ catalyst with fixed Ni surface density: Pretreatment effect on catalyst structure and catalytic activity

Journal:	<i>Catalysis Science & Technology</i>
Manuscript ID	CY-ART-08-2023-001103.R1
Article Type:	Paper
Date Submitted by the Author:	26-Oct-2023
Complete List of Authors:	<p>Lee, Kyung Min; Stony Brook University, Materials Science and Chemical Engineering</p> <p>Kim, Byeongseok; Stony Brook University, Materials Science and Chemical Engineering</p> <p>Lee, Juwon; Stony Brook University, Materials Science and Chemical Engineering</p> <p>Kwon, Gihan; Brookhaven National Laboratory, Photon Science Division - National Synchrotron Light Source II</p> <p>Yoon, Kwangsuk; Hanyang University</p> <p>Song, Hocheol ; Hanyang University</p> <p>Min, Kyung Hoon ; Inha University</p> <p>Shim, Sang Eun; Inha University, Chemical Engineering</p> <p>Hwang, Sungwon; Inha University, Department of Chemistry and Chemical Engineering;</p> <p>Kim, Tae Jin; Stony Brook University, Materials Science and Chemical Engineering</p>

ARTICLE

NO reduction by CO over NiO_x/CeO₂ catalyst with fixed Ni surface density: Pretreatment effect on catalyst structure and catalytic activity

Received 00th January 20xx,
Accepted 00th January 20xx

DOI: 10.1039/x0xx00000x

Kyung-Min Lee^{†,a}, Byeongseok Kim^{†,a,b}, Juwon Lee^{a,b}, Gihan Kwon^c, Kwangsuk Yoon^d, Hocheol Song^d, Kyung Hoon Min^b, Sang Eun Shim^b, Sungwon Hwang^b, and Taejin Kim^{*,a}

NiO_x/CeO₂ catalysts have shown promising results in various catalytic reaction including NO reduction by CO reaction. In this study, we investigated the effect of oxidation and reduction treatment on the NO reduction by CO reaction of pretreated NiO_x/CeO₂ catalysts. A series of oxidized and reduced supported NiO_x catalysts were synthesized by two steps: (1) Pretreatment CeO₂ supports with different temperature (400, 500, and 700 °C) under oxidizing and reducing conditions and (2) Synthesis of NiO_x/CeO₂ catalysts by an incipient wetness impregnation method (IWI) with a fixed surface density of 5.3 Ni/nm² under the specific conditions (oxidation/reduction) applied during the CeO₂ treatment. The prepared catalysts were characterized via BET, ICP/OES, Raman, XPS, and XRD to understand physicochemical properties. The results showed that as the pretreatment temperature increased, physicochemical properties of NiO_x/CeO₂ catalysts were changed: decreased specific surface area (SSA), decreased oxygen vacancy/defect site, and increased crystallite size. The oxidized NiO_x/CeO₂ catalyst at lower pretreatment temperature performed the better catalytic activity, indicating that the physicochemical properties of the catalysts were key factors to enhance the catalytic activity. To understand intermediate species and reaction mechanism during the NO reduction by CO reaction, in situ DRIFTS study was performed and possible reaction mechanism was also discussed.

1. Introduction

Bulk and supported nickel oxide (NiO_x) or nickel (Ni) catalysts have been applied to diverse chemical reactions (e.g., CO-PROX,¹ HER,² Selective hydrazine decomposition,³ CO oxidation,⁴ Methanol steam reforming,⁵ Dry reforming,⁶ and NO reduction by CO^{7–11}) due to their low cost and high activity. It has been reported that particle size and morphologies of Ni are related to the catalytic performance, such as methane decomposition into H₂ and carbon nanofilaments.¹² In addition to surface Ni species, support materials can also influence the reactant activation, stability, and selectivity. Among several support materials, ceria (CeO₂) or CeO₂-based materials has been used extensively, because of the easy generation of oxygen vacancies, high oxygen mobility, and strong oxygen

storage/release capacity (OSC) in the redox cycle (Ce³⁺/Ce⁴⁺).^{13–15} Y. Wang et al. reported that NiO/CeO₂ catalysts exhibited higher catalytic activity for NO reduction by CO reaction than that of NiO/γ-Al₂O₃ and NiO/TiO₂ catalysts, due to synergetic effect of nickel and ceria resulted from easily reduced oxygen species on NiO/CeO₂ surface.⁷ I. Iglesias et al., compared Ni/CeO₂ and Ni/Ce_{0.85}Zr_{0.15}O₂ catalysts to understand the effect of Zr on the catalytic property for CO₂ methanation reaction.¹⁶ The authors concluded that Ni/Ce_{0.85}Zr_{0.15}O₂ catalysts showed higher activity and stability than these of Ni/CeO₂, due to the higher oxygen mobility, surface species reducibility, and Ni dispersion. In previous studies, we reported that loading of NiO_x and pre-treatment conditions can affect the physicochemical properties (i.e., specific surface area (SSA), crystallite size, and defect sites) of NiO_x/CeO₂ and catalytic activity for NO reduction by CO.^{10,11} It was also reported that with increasing reduction temperatures, the SSA (m²/g) and surface density (# of atoms/nm²) were decreased and increased, respectively, using the same Ni wt%, ~10wt%, on NiO_x/CeO₂ samples. To study a molecular structure (i.e., monolayer) and compare a catalytic activity with different catalysts, surface density of surface species has been applied instead of using surface species wt%.^{17–20} T. C. Peck et al., reported that bulk oxide surface species were not observed up to 3.87 Fe/nm² and 1.22 Co/nm² for the series of FeO_x/CeO₂ and CoO_x/CeO₂ catalysts, respectively.¹⁸ The authors also observed that microcrystalline

^a Materials Science and Chemical Engineering Department, Stony Brook University, Stony Brook, NY, 11794, U.S.A

^b Department of Chemistry and Chemical Engineering, Education and Research Center for Smart Energy and Materials, Inha University, Incheon, 22212, South Korea

^c National Synchrotron Light Source II, Brookhaven National Laboratory, Upton, NY 11973, U.S.A

^d Department of Earth Resources and Environmental Engineering, Hanyang University, Seoul 04763, Republic of Korea

[†] co-first author, * corresponding author

Corresponding Author: *TJK: Materials Science and Chemical Engineering Department, Stony Brook University, Stony Brook, NY 11794, taejin.kim@stonybrook.edu

surface species on $\text{FeO}_x/\text{CeO}_2$ (5.4 Fe/nm^2) and $\text{CoO}_x/\text{CeO}_2$ (3.57 Co/nm^2) showed higher catalytic activity, while decreased areal activity was obtained at lower or beyond the surface densities. T. Kim et al., studied the structure-activity relationship for methanol dehydration reaction over the series of metal oxide (i.e., TiO_2 , Nb_2O_5 , Al_2O_3 , and ZrO_2) supported WO_x catalysts and reported that monolayer coverage surface density ($\sim 4.5 \text{ W/nm}^2$) could be independent on the supports.²⁰ In the case of the catalytic activity, however, it was depended on the specific oxide supports due to the different cation electronegativity.

Several researchers have investigated the effect of oxidation states of metal on their catalytic activity. S. Vivek et al., synthesized bimetallic copper and nickel nanoparticles and investigated the effect of oxidation states of Cu-Ni bimetallic on the catalytic activity and electrochemical properties.²¹ The authors reported that increased oxidation states of nickel and copper can enhance the catalytic activity. Wu et al., designed partially oxidized Ni/CeO_2 catalysts for steam methane reforming (SMR) reaction.²² Especially, the author calculated the oxidation state of Ni to improve SMR reaction by density functional theory (DFT) calculations. Based on DFT calculations, the author found that the oxidation state of Ni could affect the activity and stability of Ni/CeO_2 catalysts for SMR reaction and partially oxidized $\text{Ni}_4\text{O/CeO}_2$ catalyst showed high activity and good stability which were verified experimentally. S. D. Senanayake et al., studied the interaction between Ni atom and $\text{CeO}_2(111)$ surfaces over $\text{Ni-CeO}_2(111)$ catalysts for water-gas shift (WGS) and CO methanation reactions using X-ray and ultraviolet photoelectron spectroscopies.²³ The authors found that Ni species remain metallic state at 300K, while CeO_2 substrate was partially reduced with the formation of Ni^{2+} at 500–800K under WGS and CO methanation reactions. It was claimed that presence of metallic Ni species can promote strong interaction between chemisorbed CO and the admetal at 300 K. J. Carrasco et al., also investigated the interaction between Ni species and $\text{CeO}_2(111)$ surfaces to analyze charge transfer, oxidation states, and perturbation in the Ni density-of-states by DFT calculations.²⁴ They also compared adsorption of CO and C on the Ni_n ($n=1$ and 4) particles, because the formation of coke layers on the surface during the methanation reaction affect to the catalytic performance. The authors found that methanation activity closely related to the oxidation states of Ni and $\text{Ni/CeO}_2(111)$ showed less likely to coke formation. Although several studies have reported oxidation state effects on catalytic activity, however, direct comparison between oxidized and reduced catalysts for physicochemical properties and catalytic activity was still unclear.

In current work, the NO reduction by CO reaction over oxidized and reduced NiO_x supported on CeO_2 catalysts was investigated to understand the relationship between catalyst synthesis conditions and the physicochemical properties of the catalysts as well as a catalytic performance. Since the Ni surface density should be affected by support treatment with same Ni loading (i.e., higher treatment temperature and higher Ni surface density), for the comparison purpose, it was

fixed as 5.3 Ni/nm^2 . The physicochemical properties of the prepared catalysts were analyzed by Brunauer-Emmett-Teller (BET) technique, inductively coupled plasma/optical emission spectroscopy (ICP/OES), Raman (Visible and UV), X-ray photoelectron spectroscopy (XPS), and synchrotron X-ray diffraction (S-XRD) spectroscopy. Furthermore, to evaluate catalytic activity and understand the intermediate species during the NO reduction by CO, the gas chromatography (GC) and diffuse reflectance infrared Fourier transform spectroscopy (DRIFTS) were applied.

2. Experimental section

2.1 Catalyst synthesis

For oxidized and reduced $\text{NiO}_x/\text{CeO}_2$ catalysts, the two-step synthesis method was applied. First, as-received bulk CeO_2 (HAS 5, Rhodia) was pretreated (oxidizing and reducing) at different temperature (400, 500 and 700 °C) for 6 hrs (oxidation, dry air, 20% oxygen and 80% nitrogen, total flow rate of 100 ml min^{-1} , Airgas) or 3 hrs (reduction, 5% H_2 balanced with N_2 , total flow rate of 50 ml min^{-1} , Airgas) before being used as support materials for the $\text{NiO}_x/\text{CeO}_2$ catalysts.

The supported nickel oxide (NiO_x) catalysts were synthesized with a fixed surface density of 5.3 Ni/nm^2 using incipient wetness impregnation (IWI) method. The various concentrations of nickel (II) nitrate hexahydrate (98% $\text{Ni}(\text{NO}_3)_2 \cdot 6\text{H}_2\text{O}$, Alfa Aesar) were dissolved in de-ionized water to make precursor solutions and then the precursor solution was dropped on to pretreated CeO_2 powder while mixing constantly. After impregnation, the mixture was dried at room temperature for 12 hrs. The dried sample was transported to a combustion boat and further dried at 120 °C under flowing air (dry air, 20% oxygen and 80% nitrogen, total flow rate of 100 ml min^{-1} , Airgas) inside a tube furnace (Lindberg/Blue Mini-Mite, Thermo) for 12 hrs. Finally, the catalysts were subsequently treated in air (dry air, 20% oxygen and 80% nitrogen, total flow rate of 100 ml min^{-1} , Airgas) at different temperature (400, 500, and 700 °C) for 6 hrs to complete the oxidation process and sieved ($425 \mu\text{m}$, Fieldmaser). The synthesized CeO_2 supported nickel oxide catalysts were denoted as $5.3 \text{ NiO}_x/\text{CeO}_2\text{-400Oxi}$, $5.3 \text{ NiO}_x/\text{CeO}_2\text{-500Oxi}$, and $5.3 \text{ NiO}_x/\text{CeO}_2\text{-700Oxi}$. The reduced samples were also dried using the same method as described above and the catalysts with a fixed surface density (5.3 Ni/nm^2) were first pretreated under N_2 (UHP, 100 ml min^{-1} , Airgas) atmosphere at 400 °C for 30 min and then reduced in H_2 flow (5 vol % H_2 balanced with N_2 , total flow rate of 50 ml min^{-1} , Airgas) at different temperature (400, 500, and 700 °C) for 3 hrs. The reduced catalysts were denoted as $5.3 \text{ NiO}_x/\text{CeO}_2\text{-400R}$, $5.3 \text{ NiO}_x/\text{CeO}_2\text{-500R}$ and $5.3 \text{ NiO}_x/\text{CeO}_2\text{-700R}$.

2.2 Catalyst characterization

The specific surface area (SSA) and average pore volume of catalysts were calculated from nitrogen adsorption and desorption isotherms (Micromeritics ASAP 1010) using multipoint BET and BJH methods, respectively. Prior to analysis, the catalysts were degassed at 300 °C for 4 hrs under

vacuum to remove moistures, impurities and volatiles. To determine the Ni content in the $\text{NiO}_x/\text{CeO}_2$ catalysts, the concentration of Ni was analyzed using ICP/OES (Optima 5300DV, PerkinElmer). Prior to the analysis of ICP/OES, the catalysts were pretreated with 0.01 g of catalyst and 10 mL of nitric acid (70% HNO_3) using a microwave digestion system (ETHOS TC, Milestone). Molecular structure and bonding vibrations of supported NiO_x catalysts were obtained via Raman spectroscopy. Raman spectra were collected with visible (532 nm, Horiba Raman spectrometer) laser (laser power = 100 mW) and UV (325 nm, Renishaw inVia Raman microscope) laser (laser power = 25 mW) under ambient condition. The visible Raman spectra were collected in the 200–1400 cm^{-1} Raman shift regions and UV Raman spectra were collected in the 350–1500 cm^{-1} . For both visible and UV Raman spectra, the acquisition time was 10 seconds, and the final spectrum was accumulated from 60 scans. XPS analysis was performed to investigate the surface elemental composition and chemical state of prepared samples using K-alpha (Thermo Scientific, USA). XPS data were obtained using mono-chromated Al-K α radiation ($h\nu = 1486.6$ eV). To obtain high energy X-ray diffraction pattern, powder samples were loaded in polyimide (1mm OD Kapton) tubes sealed with clay. The diffraction patterns were obtained at 28-ID-1 PDF beamline (74.53 keV, $\lambda = 0.16635$ Å) at National Synchrotron Light Source II (NSLS-II) at Brookhaven National Laboratory (BNL). Dioptas was used to obtain one-dimensional (1D) data from the two-dimensional (2D) scattering pattern.

2.3 Catalyst activity test

The gas phase reactions were performed in a fixed bed quartz reactor (OD 9.6 mm, ID 7 mm) packed with sieved catalyst powder (40 mg) at temperature of 25–500 °C under atmosphere pressure. For experiment, the catalyst was loaded into the quartz reactor and held in place by quartz wool. Flow rates were measured by mass flow controllers (SLA5800 Series, Brooks Instrument) and temperature was monitored by a K-type thermocouple (Omega). Reaction products were identified and analyzed by TRACE™ 1300 GC (Thermo Scientific) containing a capillary column (Carboxen® 1010 PLOT) equipped with the thermal conductivity detector (TCD). Before the activity test, the prepared catalysts were pretreated at 400 °C in He (30 mL min^{-1}) for 30 mins with ramping rate of 10 °C min^{-1} . For the NO reduction by CO reaction, the gases mixtures were 5% NO (20 mL min^{-1} of 10% NO with He balance, Airgas) and 5% CO (20 mL min^{-1} of 10% CO with He balance, General Welding). The total flow rate was 40 mL min^{-1} in all experiments and a reaction temperature was increased up to 500 °C with ramping rate of 1 °C min^{-1} .

2.4 In-situ Diffuse Reflectance Infrared Fourier Transform Spectroscopy (in-situ DRIFTS)

The *in-situ* DRIFTS experiments were carried out with a Thermo Scientific Nicolet iS10 FT-IR (4 cm^{-1} spectral resolution, 32 average scans) and a Harrick Praying Mantis chamber. The

catalyst sample was first pretreated at 400 °C in flowing He (UHP, 30 mL min^{-1}) for 30 min. After pretreatment, the sample was cooled to room temperature under He flowing and a background spectrum was taken. The DRIFTS spectra were collected at different reaction temperatures, room temperature to 500 °C, with the gas mixtures of 5% NO (20 mL min^{-1} of 10% NO with He balance) and 5% CO (20 mL min^{-1} of 10% CO with He balance). To further study the formation of intermediate species in addition to the gas phase products, the DRIFTS spectra with increasing exposure time (2–30 min) at 170 °C were also collected at the following conditions: (1) CO pre-adsorption and NO reaction with CO pre-treated sample, (2) NO pre-adsorption and CO reaction with NO pre-treated sample, and (3) NO and CO co-adsorption.

3. Results

3.1 Catalytic activity test of NO reduction by CO

Fig. 1 and 2 showed the catalytic activity results of the oxidized and reduced 5.3 $\text{NiO}_x/\text{CeO}_2$ catalysts for the NO reduction by CO reaction as a function of reaction temperatures. For all samples, both NO and CO conversion were increased with an increasing of the reaction temperatures. In the case of oxidized 5.3 $\text{NiO}_x/\text{CeO}_2$ catalysts, NO conversion was slightly decreased with increasing synthesis temperatures, while CO conversions were significantly affected by the synthesis temperatures as shown in Fig. 1(a) and (b). It was also noticed that NO conversion was higher than that of CO conversion under the experimental conditions. As shown in Fig. 2(a) and (b), reduced samples showed similar trends (higher reduction temperatures lower NO and CO conversions) with oxidized samples. Similar to the oxidized samples, the reduced samples also showed a higher NO conversion than CO conversion at > 150 °C. Among the tested oxidized and reduced samples, 5.3 $\text{NiO}_x/\text{CeO}_2$ -700R showed the lowest catalytic activity (62% for NO conversion, 44% for CO conversion at 500 °C). Overall, the oxidized and reduced $\text{NiO}_x/\text{CeO}_2$ catalysts showed the decreased catalytic activities with increasing treatment temperature and the effect of pretreatment on the NO reduction by CO reaction over supported NiO_x catalysts shows the following trend: (1) NO conversion: 400Oxi \approx 500Oxi > 400R \approx 500R \approx 700Oxi >> 700R. (2) CO conversion: 400Oxi > 500Oxi > 400R > 500R > 700Oxi >> 700R. It should be noted that the treatment temperatures had a greater effect on the CO conversion than the NO conversion even at the mild oxidation and reduction temperatures, such as 400 °C and 500 °C. The N_2 and N_2O selectivity were also evaluated, and results are shown in Fig. 1(c) and (d) and Fig. 2(c) and (d). As shown in selectivity results, N_2O was produced at lower temperature, while N_2 selectivity was increased with increasing reaction temperatures. The detailed reaction mechanism of intermediate N_2O species will be further discussed in the DRIFTS section.

3.2 Physical properties of the catalysts

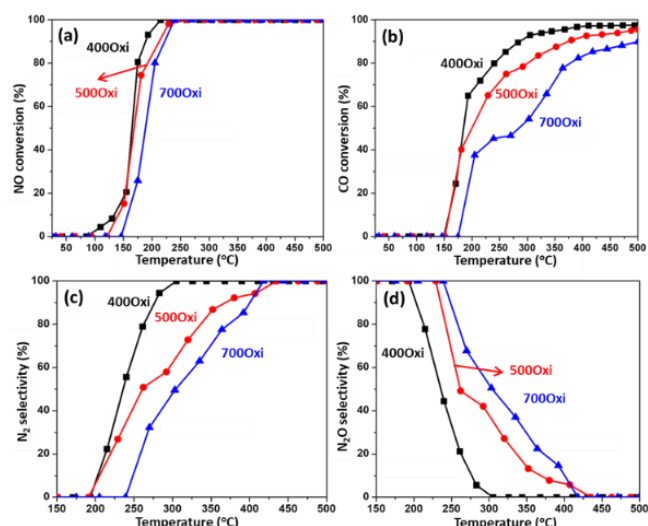


Fig. 1 Catalytic activity of the oxidized 5.3 NiO_x/CeO₂ catalysts for NO reduction by CO reaction at different reaction temperatures. (a) NO conversion, (b) CO conversion, (c) N₂ selectivity, and (d) N₂O selectivity. Reaction conditions: 5% NO and 5% CO balanced with helium, total flow rate = 40 ml min⁻¹, GHSV = 60,000 ml g⁻¹ h⁻¹.

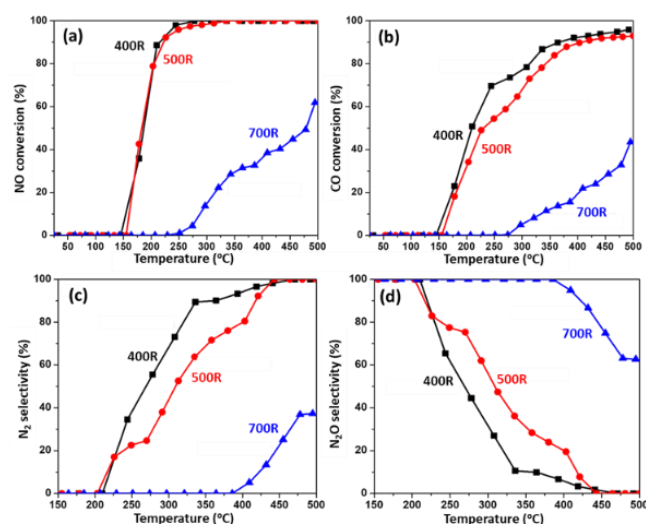


Fig. 2 Catalytic activity of the reduced 5.3 NiO_x/CeO₂ catalysts for NO reduction by CO reaction at different reaction temperatures. (a) NO conversion, (b) CO conversion, (c) N₂ selectivity, and (d) N₂O selectivity. Reaction conditions: 5% NO and 5% CO balanced with helium, total flow rate = 40 ml min⁻¹, GHSV = 60,000 ml g⁻¹ h⁻¹.

To understand relationship between physical properties and catalytic activity of the prepared catalysts, the BET specific surface area (SSA), total pore volume, and average pore diameter were investigated by the nitrogen adsorption and desorption isotherm. The isotherm curves of 400 °C and 500 °C pretreated samples (oxidized and reduced) exhibited type IV isotherm with a H1-type hysteresis loop shape (Fig. 3(a) and (b)), implying that catalysts consist of mesoporous structure.^{25,26} The 700 °C pretreated samples (700Oxi and 700R), however, showed type V isotherms with a H3 hysteresis loop, indicating pores and relatively large pore size. (Fig. 3 (a) and (b)) Compared to the bulk CeO₂ that contains a mesopore structure as reported in our previous research,¹¹ the oxidized

and reduced NiO_x/CeO₂ catalysts at 400 °C and 500 °C showed similar shape of isotherm curves, indicating that the mesoporous structure of CeO₂ was maintained even after introducing NiO_x (5.3 Ni/nm²) and thermal treatment. The specific surface area (SSA), Ni wt%, surface density (SD) from NiO_x/CeO₂ sample's SSA, total pore volume, and average pore diameter are listed in Table 1. It is noted that to fix surface density (5.3 Ni atoms/nm², as a target SD) of supported NiO_x catalysts, Ni weight percents were calculated based on the SSA of pretreated CeO₂ supports. As shown in Table 1, experimentally obtained SD values, 5.6–6.8 Ni/nm², were similar or higher than that of the target value, 5.3 Ni/nm². The Ni wt% and SD values of oxidized and reduced samples were also measured by ICP-OES and the results are included in Table 1. Compared to the bulk CeO₂ (as-received), the SSA of pretreated NiO_x/CeO₂ decreased with increasing pretreatment temperature, while pore diameter increased due to sintering

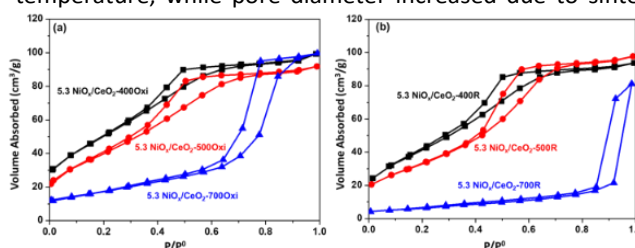


Fig. 3 N₂ adsorption-desorption isotherms of the (a) oxidized and (b) reduced 5.3 NiO_x/CeO₂ catalysts.

of CeO₂ under high treatment temperature, especially at 700 °C.

3.3 Raman spectroscopy

For investigating detailed molecular structure of oxidized and reduced 5.3 NiO_x/CeO₂ catalysts, Raman spectroscopy was performed. As shown in Fig. 4(I) and (II), the visible Raman spectra showed dominant peak at ~460 cm⁻¹, which corresponded to the intrinsic F_{2g} symmetric vibrational mode of fluorite CeO₂, with weak bands at ~236 cm⁻¹ and ~600 cm⁻¹, due to second-order transverse acoustic (2TA) mode and oxygen vacancy/defect induced (D) mode, respectively.^{27–30} Based on our previous work,¹¹ the broad peak at 540 cm⁻¹ could be assigned to NiO_x related band. For both oxidized and reduced catalysts, the F_{2g} peak (~460 cm⁻¹) became narrower and sharper (decreased a full width at half maximum (FWHM)) with increasing pretreatment temperature, due to increased crystallinity. The peak position of F_{2g} was slightly shifted (461 to 468 cm⁻¹ (Oxi) and 469 cm⁻¹ (Red)) with increasing pretreatment temperature, while the peak positions of D band (~600 cm⁻¹) for both oxidized and reduced samples were not shifted. Based on visible Raman spectra results of oxidized and reduced catalysts, the concentration of oxygen vacancies (N) can be calculated using the spatial correlation model from the relationship between grain size (d_g) and correlation length (average distance between two lattice defects, L). The detailed equations are provided as follows:

Table 1 Specific surface area, surface density, total pore volume, and average pore size of the NiO_x/CeO₂ catalysts

Sample*	SSA (m ² /g)	Ni wt (%)	SD** (Ni/nm ²)	Ni wt*** (%)	SD**** (Ni/nm ²)	Total pore volume (cm ³ /g)	Average pore diameter (nm)
Bulk CeO ₂ *****	216	-	-	-	-	0.16	1.5
5.3 NiO _x /CeO ₂ -400Oxi	180	9.9	5.6	9.42	5.37	0.15	1.7
5.3 NiO _x /CeO ₂ -500Oxi	150	9.4	6.4	8.46	5.78	0.14	1.9
5.3 NiO _x /CeO ₂ -700Oxi	59	3.9	6.8	3.35	5.83	0.15	5.2
5.3 NiO _x /CeO ₂ -400R	158	9.8	6.4	8.45	5.49	0.14	1.8
5.3 NiO _x /CeO ₂ -500R	129	8.2	5.7	7.62	6.06	0.15	2.3
5.3 NiO _x /CeO ₂ -700R	22	1.4	6.5	1.35	6.29	0.12	11.4

* 5.3 is the surface density of Ni (Ni/nm²) using support's SSA = $\frac{W_{Ni} \times 6.02 \times 10^{23} \times \frac{1}{M_{Ni}}}{S \times (1 - \frac{W_{Ni}}{100}) \times 10^{18}}$ where W_{Ni} is the weight percentage of Ni, M_{Ni} is the atomic weight of Ni (58.7 g/mol), and S is the SSA of the oxidized or reduced CeO₂ sample.

** surface density of Ni (Ni/nm²) using sample's SSA = $\frac{W_{Ni} \times 6.02 \times 10^{23} \times \frac{1}{M_{Ni}}}{S \times 10^{18}}$ where W_{Ni} is the weight percentage of Ni, M_{Ni} is the atomic weight of Ni (58.7 g/mol), and S is the SSA of the oxidized or reduced 5.3 NiO_x/CeO₂ sample.

*** Ni weight percent obtained by ICP/OES.

Table 2 The grain size (d_g), correlation length (L), concentration of oxygen vacancies (N), and defect ratio (I₀/I_{F2g}) of the oxidized and reduced 5.3 NiO_x/CeO₂ catalysts.

Catalyst	Grain size of CeO2 (d _g , nm)	Correlating length (L, nm)	Concentration of oxygen vacancies (N x 10 ⁻²¹ , cm ⁻³)	Defect ratio (I ₀ /I _{F2g})
Bulk CeO ₂	2.77	0.42	3.24	1.06*
5.3 NiO _x /CeO ₂ -400Oxi	3.07	0.43	2.93	0.91
5.3 NiO _x /CeO ₂ -500Oxi	3.96	0.47	2.28	0.74
5.3 NiO _x /CeO ₂ -700Oxi	7.63	0.59	1.15	0.40
5.3 NiO _x /CeO ₂ -400R	3.63	0.46	2.49	0.56
5.3 NiO _x /CeO ₂ -500R	4.34	0.49	2.08	0.33
5.3 NiO _x /CeO ₂ -700R	17.25	0.78	0.49	0.18

* Results from reference [35]

**** surface density of Ni (Ni/nm²) using sample's SSA = $\frac{W_{Ni} \times 6.02 \times 10^{23} \times \frac{1}{M_{Ni}}}{S \times 10^{18}}$, where the W_{Ni} was obtained by ICP/OES.

***** results from reference [11]

$$\Gamma = \frac{51.8}{d_g} + 5 \quad \text{or} \quad d_g = \frac{51.8}{(\Gamma - 5)} \tag{1}$$

$$L(nm) = \sqrt[3]{\left(\frac{\alpha}{2d_g}\right)^2 \left[(d_g - 2\alpha)^3 + 4d_g^2\alpha\right]} \tag{2}$$

$$N = \frac{3}{4\pi L^3} \tag{3}$$

Where Γ is the HWHM of the F_{2g} peak (~ 460 cm⁻¹) of CeO₂, d_g is the grain size of CeO₂, L is the correlation length of CeO₂, and α is the radius (0.34 nm) of CeO₂ units.^{28,30} As shown in Table 2, the grain size of CeO₂ (d_g) and correlation length (L) were increased with increasing temperatures, while the concentrations of oxygen vacancies (N) were decreased with increasing temperatures. The observed results show a similar trend of the SSA values shown in Table 1.

It was reported that UV Raman can provide more detail information of defect sites of CeO₂, due to the resonance Raman effect result from strong absorption CeO₂ in the UV region.^{31–33} To better understand oxygen vacancies (or defect sites) of CeO₂ supported NiO_x catalysts, UV Raman spectra were collected. Fig. 5 displays UV Raman spectra of oxidized and reduced 5.3 NiO_x/CeO₂ catalysts. Compared to visible Raman spectra, UV Raman spectra showed new peak at ~ 1180 cm⁻¹, which could be ascribed to second-order longitudinal (2LO) mode.^{29,30} It is worthwhile to note that the peak intensity of 2LO band (~1180 cm⁻¹) as strong as the F_{2g} band (~460 cm⁻¹), due to enhancement of the longitudinal (LO) overtones under UV region.³⁴ Furthermore, the peak position of 2LO band was shifted from 1140 cm⁻¹ to 1180 cm⁻¹ as the oxidation temperature increased, indicating that the Ce-O bond became stronger with increasing oxidation temperature.³ In the case of the reduced samples, however,

the 2LO bands were not much affected by the reduction temperatures. (Fig. 5(II)) As shown in the insets of Fig. 5, the relative intensity ratio of defect vibration (I_D/I_{F2g}) for both oxidized and reduced catalysts decreased with increasing pretreatment temperatures, suggesting that thermal effect induced decrease in oxygen vacancy/defect sites. For both concentration of oxygen vacancies (N) and defect ratio (I_D/I_{F2g}), as shown in Table 2, the values for both oxidized and reduced catalysts decreased with increasing treatment temperatures. Although the trends of defect ratio were similar, however, reduced catalysts showed the lower defect concentration than those of the oxidized samples, indicating that both treatment temperature and gas compositions were affected to oxygen vacancies and defect sites.

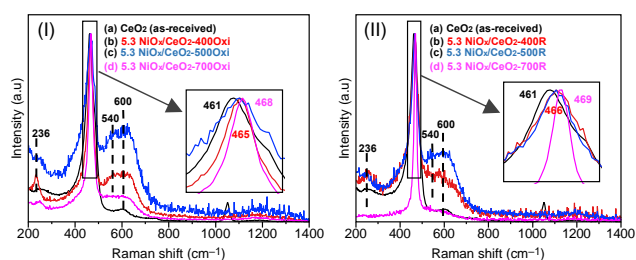


Fig. 4 Visible Raman spectra of (I) oxidized 5.3 NiO_x/CeO₂ ((a) CeO₂, (b) 5.3 NiO_x/CeO₂-400Oxi, (c) 5.3 NiO_x/CeO₂-500Oxi, and (d) 5.3 NiO_x/CeO₂-700Oxi), (II) reduced 5.3 NiO_x/CeO₂ ((a) CeO₂, (b) 5.3 NiO_x/CeO₂-400R, (c) 5.3 NiO_x/CeO₂-500R, and (d) 5.3 NiO_x/CeO₂-700R).

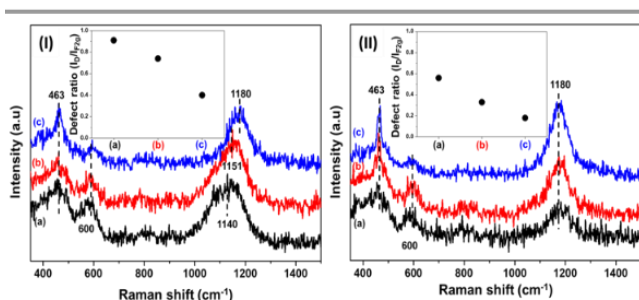


Fig. 5 UV Raman spectra of (I) oxidized 5.3 NiO_x/CeO₂ ((a) 5.3 NiO_x/CeO₂-400Oxi, (b) 5.3 NiO_x/CeO₂-500Oxi, and (c) 5.3 NiO_x/CeO₂-700Oxi), (II) reduced 5.3 NiO_x/CeO₂ ((a) 5.3 NiO_x/CeO₂-400R, (b) 5.3 NiO_x/CeO₂-500R, and (c) 5.3 NiO_x/CeO₂-700R). Inset: defect ratio of oxidized and reduced catalysts. Defect ratio = I_D (600 cm⁻¹)/ I_{F2g} (464 cm⁻¹).

3.4 X-ray photoelectron spectroscopy (XPS)

XPS analysis was performed to illuminate oxidation states and surface composition of prepared catalysts. Fig. 6(a) shows deconvoluted the core level Ce 3d XPS spectra in the 925–875 eV for 5.3 NiO_x/CeO₂ catalysts oxidized at 400, 500, and 700 °C. In this range, the Ce 3d spectra consist of the u band (3d_{5/2}) and v band (3d_{3/2}), which are further resolved into ten sub-peaks ($u_0, u, u', u'', u''', v_0, v, v', v'',$ and v''').^{35,36} The four sub-peaks, v_0 (~880.11 eV), v' (~882.54 eV), u_0 (~899.20 eV), and u' (~903.51 eV), correspond to Ce³⁺ species, while the remaining six sub-peaks, v (~882.47 eV), v'' (~888.87 eV), v''' (~898.27 eV), u (~903.51 eV), u'' (~907.47 eV), and u''' (~916.74 eV), are related to Ce⁴⁺ species and peaks shifts between samples were

rarely observed. These are highlighted in Fig. 6(a) and (b), with the sub-peaks corresponding to Ce³⁺ shown in red and sub-peaks corresponding to Ce⁴⁺ in blue. Calculating the area ratios of these sub-peaks allows us to assess the relative content of Ce³⁺

on the surface of the catalysts. Table 3 provides the values obtained by dividing Ce³⁺ area by the sum of Ce³⁺ and Ce⁴⁺ areas. The Ce³⁺ ratio in 5.3 NiO_x/CeO₂-400Oxi (24%) and 5.3 NiO_x/CeO₂-500Oxi (24%) samples exhibited similar values. However, in the case of 5.3 NiO_x/CeO₂-700Oxi, the Ce³⁺ ratio decreased to 18%. The reduced catalysts were also subjected to peak deconvolution in the same manner (Fig. 6(b)), and the Ce³⁺ ratio was determined (Table 3). In the reduced catalysts, the Ce³⁺ ratio was continuously decreased with increasing reduction temperatures.

In the case of the Ni 2p_{3/2}, three distinct sub-peaks, located at 853.5, 855.8, and 861.5 eV, were observed, which are attributed to Ni²⁺ in NiO, Ni³⁺, and satellite peaks, respectively (Fig. 6(c) and (d)).^{37,38} It is noted that only the Ni 2p_{3/2} region was analyzed because of the overlap between the Ce 3d peak and the Ni 2p_{1/2} peak. The samples subjected to oxidized show a slight increase in the peak at approximately 855.8 eV peak assigned to Ni³⁺ compared to the 853.5 eV peak assigned to Ni²⁺ at both 400 and 500 °C. The catalyst oxidized at 700 °C exhibits a low Ni content, making it challenging to achieve high intensity, but it appears to have a high Ni³⁺ content compared to the Ni²⁺. To quantitatively assess the change in the oxidation state of Ni with temperature, the area of Ni³⁺ was divided by the sum of Ni²⁺ and Ni³⁺ area (Table 3). For the oxidized catalysts, there was not a substantial difference between 400 and 500 °C, with values of 0.68 and 0.70, respectively. In the case of the reduced catalysts, it is evident that the peak at 855.8 eV increases significantly even with the temperature difference between 400 and 500 °C (Fig. 6(d)). When calculating the relative area ratio of Ni³⁺ in the same manner to the oxidized samples, it is 0.71 at 400 °C, and when treated at 500 °C, it increases to 0.83. This indicates that the oxidation state of Ni is sensitive to changes under reducing conditions. Similar to the XPS data of the 700Oxi sample, the 700R sample also exhibited low Ni peaks. Although quantifying the Ni³⁺ ratio was difficult, the intensity of the Ni³⁺ peak was relatively higher than that of Ni²⁺.

Fig. 6(e) and (f) shows deconvoluted O 1s XPS spectra in the 540–520 eV for all samples. The O 1s peak could be deconvoluted into two sub-peaks. The peak at 529.21 eV (O') corresponds to lattice oxygen, while the peak at 530.83 eV (O'') corresponds to oxygen present in absorbed species such as carbonates and hydroxyl groups.^{37,38} By calculating the area ratio of these two peaks, concentration of oxygen vacancies of catalysts surface could be obtained indirectly. In the case of oxidized catalysts, the O''/O' ratio of 5.3 NiO_x/CeO₂-400Oxi and 5.3 NiO_x/CeO₂-500Oxi both exhibit values of 1.01, showing no difference. At 700 °C, the ratio of O'' significantly decreased to 0.84. This trend aligns with the Ce³⁺/(Ce³⁺+Ce⁴⁺). For the reduced catalysts, the ratio was 1.00 for 5.3 NiO_x/CeO₂-400R, but as the heat treatment temperature increased to 500 °C (5.3 NiO_x/CeO₂-500R), it dropped to 0.90, indicating that heat

treatment temperature under reducing condition sensitively affected oxidation states of catalysts. Furthermore, at 700 °C, the O'' ratio decreased significantly to 0.64.

3.5 Powder X-ray diffraction (XRD)

To understand effect of oxidation and reduction treatment on crystalline structure of the series of NiO_x/CeO₂ catalysts, synchrotron-based X-ray diffraction (s-XRD) spectra were collected (Fig. 7). For all the supported NiO_x catalysts, the fluorite CeO₂ (□ symbol) peaks (JCPDS-ICDD Card No. 34-394) at 3.0° (111), 3.5° (200), 4.9° (220), 5.8° (311), 6.1° (222), 7.0° (400), 7.6° (331), 7.8° (420), 8.6° (422), and 9.1° (511) were clearly observed, especially at 700 °C treated samples. In addition to the fluorite CeO₂ peaks, oxidized 5.3 NiO_x/CeO₂ catalyst contained nickel oxide (Δ symbol) peaks at 3.9°, 4.5°, and 6.4°, which can be ascribed to the (111), (200), and (220) reflections of nickel oxide, respectively (JCPDS-ICDD Card No.04-0835).

As shown in inset Fig. 7(a), the intensity of nickel oxide peaks increased with increasing temperature up to 500 °C, while the peak intensity drastically decreased at 700 °C, due to relative

peaks were still remained, indicating that the nickel species were not fully reduced at 400 and 500 °C, while the 700R samples contained only metallic nickel species (Fig. 7(c)). Note

Table 3 The ratio of Ce³⁺ compared to Ce³⁺+Ce⁴⁺, the ratio of Ni³⁺ compared to Ni²⁺+Ni³⁺, and the ratio of O'' compared to O' on the surface of oxidized 5.3 NiO_x/CeO₂ and reduced 5.3 NiO_x/CeO₂

Sample	Ce ³⁺ /(Ce ³⁺ +Ce ⁴⁺) (mol/mol)	Ni ³⁺ /(Ni ²⁺ +Ni ³⁺) (mol/mol)	O''/O' (mol/mol)
5.3NiO _x /CeO ₂ -400Oxi	0.24	0.68	1.01
5.3NiO _x /CeO ₂ -500Oxi	0.24	0.70	1.01
5.3NiO _x /CeO ₂ -700Oxi	0.18	-	0.84
5.3NiO _x /CeO ₂ -400R	0.27	0.71	1.00
5.3NiO _x /CeO ₂ -500R	0.21	0.83	0.90
5.3NiO _x /CeO ₂ -700R	0.19	-	0.64

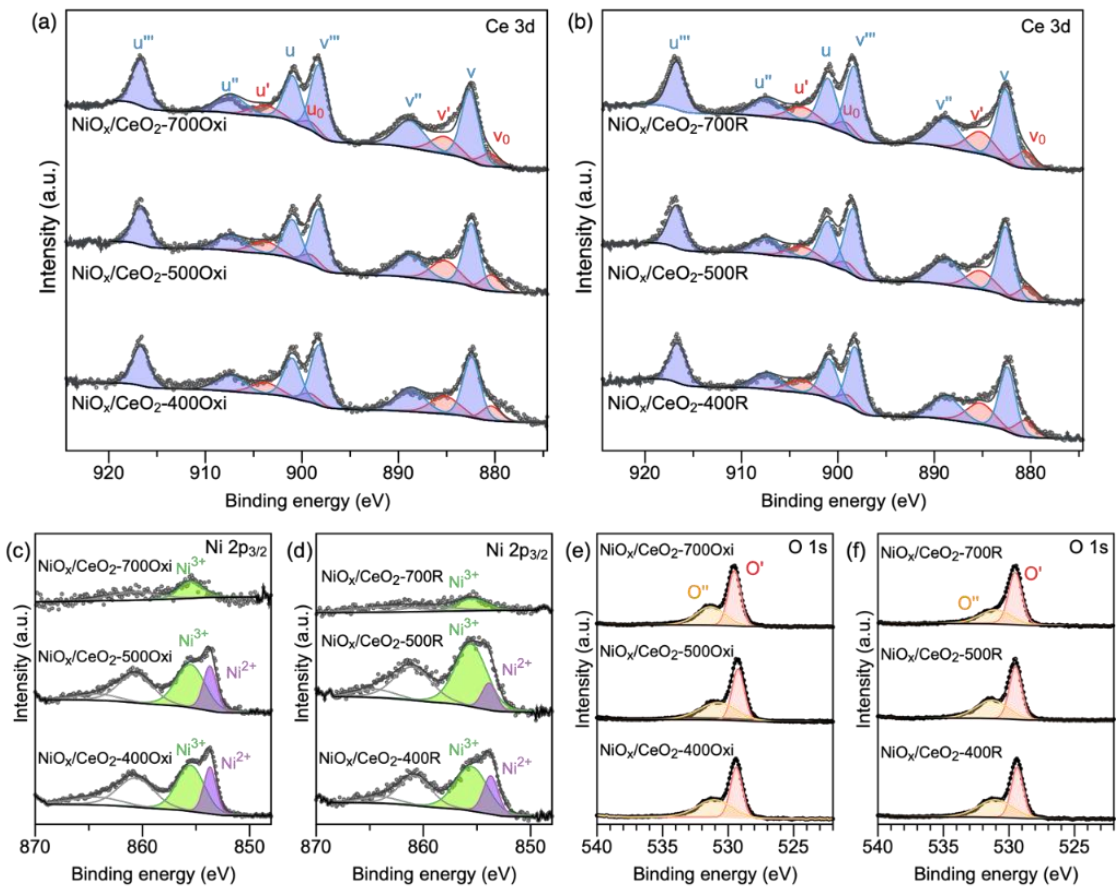


Fig. 6 Deconvoluted Ce 3d XPS spectra of (a) oxidized 5.3 NiO_x/CeO₂, (b) reduced 5.3 NiO_x/CeO₂. Deconvoluted Ni 2p_{3/2} XPS spectra of (c) oxidized 5.3 NiO_x/CeO₂, (d) reduced 5.3 NiO_x/CeO₂. Deconvoluted O 1s XPS spectra of (e) oxidized 5.3 NiO_x/CeO₂, (f) reduced 5.3 NiO_x/CeO₂.

lower Ni concentration (3.9wt%) of 5.3 NiO_x/CeO₂-700Oxi sample. For reduced 5.3 NiO_x/CeO₂ catalysts, there were new peaks (○ symbol) at 4.7°, 5.4°, 8.9°, and 9.3°, which can be ascribed to (111), (200), (311), and (222) reflections of fcc Ni (JCPDS-ICDD Card No. 04-0850 (fcc)), respectively (Fig. 7(b) and (c)). For 5.3 NiO_x/CeO₂-400R and 500R samples, nickel oxide

that Ni peak intensity was very low in the 700R sample's XRD pattern, due to a low Ni concentration (1.4wt%). For both oxidized and reduced catalysts, the CeO₂ (111) peak became sharper with increasing treatment temperatures, suggesting that the crystallite size of CeO₂ was changed as the pretreatment temperature increased. The crystallite sizes of

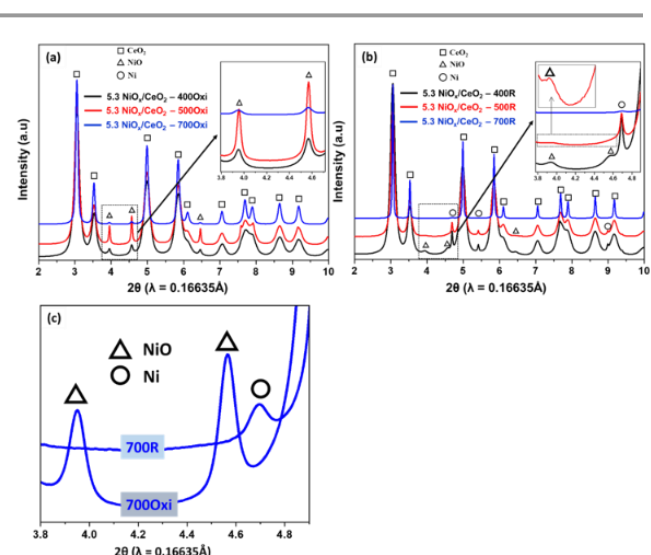


Fig. 7 XRD patterns of (a) oxidized 5.3 NiO_x/CeO₂, (b) reduced 5.3 NiO_x/CeO₂ catalysts, and (c) 700Oxi and 700R 5.3 NiO_x/CeO₂.

Table 4 CeO₂ (111) Peak position, full width half maximum (FWHM), calculated crystallite size, and lattice parameters of the oxidized and reduced 5.3 NiO_x/CeO₂ catalysts

Sample	CeO ₂ (111) Peak Position (°)	CeO ₂ (111) FWHM (°)	Crystallite size* (nm)	Lattice parameter** (Å)
5.3 NiO _x /CeO ₂ -400Oxi	3.05	0.16	5.41	5.41
5.3 NiO _x /CeO ₂ -500Oxi	3.05	0.14	6.00	5.41
5.3 NiO _x /CeO ₂ -700Oxi	3.05	0.08	11.13	5.41
5.3 NiO _x /CeO ₂ -400R	3.05	0.15	5.78	5.41
5.3 NiO _x /CeO ₂ -500R	3.05	0.12	7.12	5.41
5.3 NiO _x /CeO ₂ -700R	3.05	0.04	20.96	5.41

$$*: D = 0.9\lambda / (\beta \cdot \cos\theta)$$

$$**: a = \sqrt{h^2 + k^2 + l^2} \cdot d_{111} = \sqrt{3}d_{111}, \quad d_{111} = \frac{\lambda}{2 \cdot \sin\theta_{111}}$$

where D is the crystallite size, λ is the X-ray wavelength (0.16635 Å), β is the FWHM of the CeO₂ (111) peak, θ is the Bragg angle of the peak, a is the lattice parameter, and d is the spacing of (111) lattice planes.

CeO₂ of prepared samples were calculated using Scherrer's equation and were listed in Table 4. For both oxidized and reduced samples at 700 °C, the average CeO₂ crystallite size was

drastically increased, while the lattice parameter of CeO₂ was not changed, suggesting that the sintering at high temperature

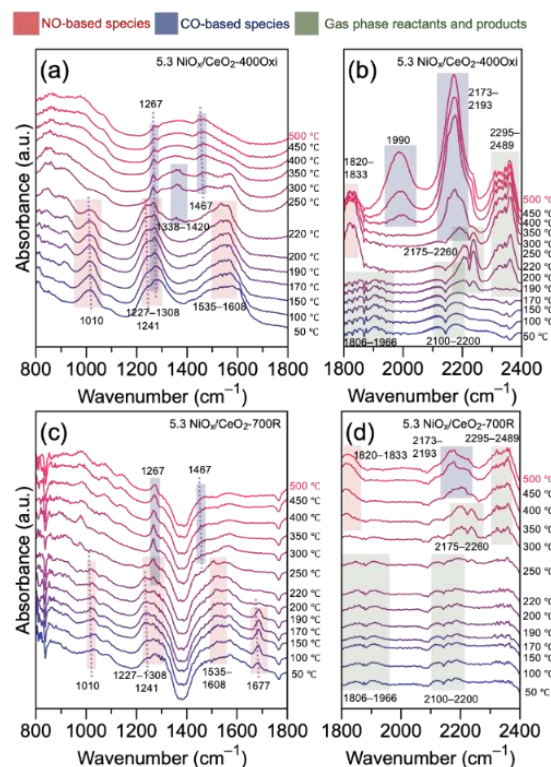


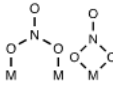
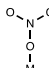
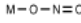
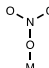
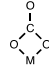
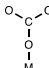
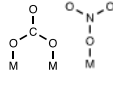
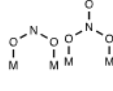
Fig. 8 *In-situ* DRIFTS of (a) 5.3 NiO_x/CeO₂-400Oxi (800–1800 cm⁻¹), (b) 5.3 NiO_x/CeO₂-400Oxi (1800–2400 cm⁻¹), (c) 5.3 NiO_x/CeO₂-700R (800–1800 cm⁻¹), and (d) 5.3 NiO_x/CeO₂-700R (1800–2400 cm⁻¹) in NO reduction by CO at different temperatures. Reaction conditions: 5% NO, 5% CO balanced with helium, temperature = 50–500 °C

induced the larger crystallites and increased crystallinity of the pretreated samples. Compared to 5.3 NiO_x/CeO₂-700Oxi catalyst (11.13 nm), reduced catalyst at 700 °C showed larger crystallite size (20.96 nm), indicating that not only treatment temperature, but also reducing condition could be enhanced sintering effect.

3.5 Diffuse reflectance infrared Fourier transform spectroscopy (DRIFTS)

When comparing the catalytic activity with oxidized and reduced catalysts, it was observed that the catalyst activity decreases as the pretreatment temperature increases (Fig. 1 and 2). Furthermore, even at the same treatment temperature, the catalyst activity was lower when treated in the reducing condition compared to the oxidizing condition. In conclusion, the catalyst exhibited the highest activity when pretreated at a relatively low temperature of 400 °C in the oxidizing condition, while the catalyst activity was lowest when pretreated at a relatively high temperature of 700 °C in the reducing condition. To investigate the interaction between the reactants (NO and CO) and catalyst surface as well as the formation of the intermediate species, *in-situ* DRIFTS analysis was performed for 5.3 NiO_x/CeO₂-400Oxi (highest activity) and 5.3 NiO_x/CeO₂-700R (lowest activity) catalysts in the temperature range of 50–500 °C. As shown in Fig. 8(a), *in-situ* DRIFTS spectra of the oxidized 5.3 NiO_x/CeO₂ sample exhibited absorbance peaks

Table 5 Peak assignments of the DRIFTS spectra

IR wavenumber (cm ⁻¹)	Assignments	Structure	Ref.
1010	Bridging bidentate nitrate, Bidentate nitrate		39, 40
1227–1308	Monodentate nitrate, Linear nitrite	 	39, 40
1241	Monodentate nitrate		41, 42
1267	Bidentate carbonate		43, 44, 45
1338–1420	Monodentate carbonate		43, 44, 45
1467	Bidentate carbonate, Monodentate nitrate		43, 44, 45
1535–1608	Bridging nitro, Bridging bidentate nitrate		39, 40
1806–1966	NO (gas phase)	N=O	39, 40
1820–1833	NO adsorbed on Ni ²⁺ or Ni ⁺	Ni ⁿ⁺ -NO	47
1990	CO adsorbed on Ni ⁺	Ni ²⁺ -CO	47
2100–2200	CO (gas phase)	C≡O	43, 46
2173–2193	CO adsorbed on Ni ²⁺	Ni ²⁺ -CO	47
2175–2260	N ₂ O	O-N≡N	8
2295–2489	CO ₂	O=C=O	46

corresponding to various NO and CO based intermediate surface species.

For the NO-based surface species, the following peaks were observed from 50 °C to 220 °C: bridging bidentate nitrate at 1010 cm⁻¹, bidentate nitrate (or linear nitrite or monodentate nitrate) in the range of 1227–1308 cm⁻¹ and monodentate nitrate (or bridging nitro or bridging bidentate nitrate) in the range of 1535–1608 cm⁻¹.^{39,40} Additionally, a minor peak at 1241 cm⁻¹ was observed, corresponding to monodentate nitrate.^{41,42} For the CO-based surface species, the following peaks were observed: bidentate carbonate at 1267 cm⁻¹ (≥150 °C), monodentate carbonate or carboxylate in the range of 1338–1420 cm⁻¹ and bidentate

carbonate at 1467 cm⁻¹ (≥ 220 °C).^{43–45} The 5.3 NiO_x/CeO₂-700R sample displayed slightly different DRIFTS spectra compared to the 5.3 NiO_x/CeO₂-400Oxi sample's results (Fig. 8(c)): (I) NO-based intermediate species' peak intensity was relatively weak, (II) Monodentate carbonate or carboxylate peak (1338–1420 cm⁻¹) was not observed, while bidentate carbonate peak appeared from 200~250 °C which was higher than that of 5.3 NiO_x/CeO₂-400Oxi one (150~170 °C).

The generation of intermediate surface species leads to the several gaseous products (Fig. 8 (b) and (d)). The weak band at 1806–1966 cm⁻¹ were attributed to gas phase NO and it disappeared at ≥ 200 °C (5.3 NiO_x/CeO₂-400Oxi) and ≥ 300 °C (5.3 NiO_x/CeO₂-700R), respectively. The gas phase CO (2100–2200 cm⁻¹) started showing at 50 °C and disappeared at >250 °C (5.3 NiO_x/CeO₂-400Oxi) and >350 °C (5.3 NiO_x/CeO₂-700R), respectively. The gas phase CO₂ peak at 2295–2489 cm⁻¹ started showing at 200 °C (5.3 NiO_x/CeO₂-400Oxi), while those of 5.3 NiO_x/CeO₂-700R appeared at 300 °C and their intensities increased as the reaction temperature increased. The N₂O intermediate surface species were also observed at 2175–2260 cm⁻¹ and appeared at 170 °C (5.3 NiO_x/CeO₂-400Oxi) and 250 °C (5.3 NiO_x/CeO₂-700R), respectively.⁸ In addition, NO and CO adsorption on surface nickel oxide was also observed: 1820–1833 cm⁻¹ (Ni⁺/Ni²⁺-NO or CO), 1990 cm⁻¹ (Ni⁺-CO), and 2173–2193 cm⁻¹ (Ni²⁺-CO), respectively.⁴⁷ It should be noted that the 5.3 NiO_x/CeO₂-700R sample contained Ni only based on the S-XRD results as shown in Fig. 8 (b) and (c). Although peak intensity of Ni⁺/Ni²⁺-NO and Ni²⁺-CO are very weak, the in-situ DRIFT result provided that Ni on 5.3 NiO_x/CeO₂-700R sample was partially oxidized during the reaction especially at > 300 °C. For 5.3 NiO_x/CeO₂-700R sample, the Ni⁺-CO peak (1990 cm⁻¹) was not observed, indicating that the CO adsorption on the surface was limited, due to lower nickel concentration and surface area. As shown in Fig. 8, the NO adsorption peak appeared at lower temperature than those of CO adsorption peak. From these results, it can be hypothesized that the NO-based surface species could be adsorbed on the active sites (Ni⁺ or Ni²⁺) at lower temperature (< 250 °C), then activated CO adsorption on the surface result in replacement NO species at higher temperature.

4. Discussion

4.1 Pretreatment effect on the physicochemical properties of NiO_x/CeO₂ catalysts

The oxidation or reduction treatment can have great impacts on the molecular structure of the supported metal catalyst, and further affect to catalytic performance. With increasing pretreatment temperature (400–700 °C), the physicochemical properties, molecular structure, and electronic structures of 5.3 NiO_x/CeO₂ catalysts were investigated by various characterizations, such as BET, ICP/OES, Raman, XPS, and XRD. Based on BET results (Table 1), it was observed that introducing NiO_x species and pretreatment with increasing temperature caused collapsing of the small pores and agglomeration of CeO₂, resulting in decreased in SSA and pore volume as well as increased pore diameter. Z. Wang et al. reported that the decreased specific surface area and

increased pore diameter of synthesized transition metal (Co, Mn, Fe, Cr, and Ni) doped ceria substrate catalysts might be due to sintering of the samples and resulting in the larger crystalline grain with increasing calcination temperature.⁴⁵ Visible and UV Raman results provided that concentrations of oxygen vacancies and defect ratio were decreased with increasing pretreatment temperature. From UV Raman spectra (Fig. 5) of both oxidized and reduced samples, 400 °C and 500 °C samples showed relatively similar peak intensity of D-band ($\sim 600\text{ cm}^{-1}$), while there is a large decrease in peak intensity of D-band for 700 °C treated samples. These results were consistent with the results of BET (decreased SSA, increased pore size), indicating that significant molecular structure changes occurred after high temperature pretreatment at 700 °C. Overall, the oxidized 5.3 NiO_x/CeO₂ samples showed higher concentration and defect ratio than those of reduced samples at corresponding pretreatment temperatures (Table 2). Recently, Yang et al., reviewed defect chemistry in CeO₂-based heterogeneous catalysis and the author claimed that these defect structures of CeO₂ plays a key role in several catalytic activities.⁴⁸ The author also introduced several strategies for introducing defects, such as metal doping, chemical reduction, size and morphology control, and X-ray or electron beam irradiation. From Visible and UV Raman results, we can possibly obtain the information of concentration of oxygen vacancies/defect sites of oxidized and reduced catalysts, which can affect the catalytic performance. In addition to defect ratio changes, visible Raman results showed that the peak position of F_{2g} was slightly shifted (blue shift, 461 to 468 cm⁻¹ (Oxi) and 469 cm⁻¹ (Red)), that is might due to disorder of oxygen species in the lattice, increasing particle size, and deficiency of Ce³⁺ species with increasing pretreatment temperature.^{3,49,50}

The surface characteristics of the synthesized catalysts were inferred based on the XPS results. Notably, both oxidized and reduced catalysts exhibited different trends in response to varying heat treatment temperatures. For the oxidized catalyst, there was no significant difference in the Ce³⁺ ratio between treatments at 400 and 500 °C. However, in the case of reduced catalysts, the Ce³⁺ ratio decreased as the reduction temperature increased from 400 °C to 500 °C, suggesting that, during heat treatment under reducing conditions, the reduction of ceria did not occur significantly. Samples treated at 700 °C exhibited similar Ce³⁺ ratios in both oxidation (18%) and reduction (19%) processes. In the case of samples subjected to oxidation, the change in the Ni³⁺ ratio was not significant when heated from 400 to 500 °C, compared to samples subjected to reduction, which clearly exhibited an increase in Ni³⁺ ratio at both 400 and 500 °C. This observation is likely due to the formation of NiOOH or Ni vacancies, which lead to the presence of Ni³⁺.⁵¹ Based on the results, it can be inferred that the introduced OH adsorbed on the nickel oxide surface, resulting in the formation of hydroxyl groups (NiOOH), leading to an increase in Ni³⁺ content. However, at 700 °C, an increase in the amount of Ni existing as Ni³⁺ was observed in both the oxidized and reduced samples, although it is not as pronounced. This suggests that the influence of Ni vacancies due to high-temperature treatment might play a role. In this experiment, it is evident that both nickel vacancy and NiOOH did not significantly impact the conversion of CO oxidation reaction

(Fig. 1 and Fig. 2). The O'' to O' transition in the oxidized sample remains similar at 400 and 500 °C but decreases at 700 °C. This could be attributed to the disappearance of surface OH groups and the reduction of oxygen vacancies. The Raman results indicate a noticeable reduction in oxygen vacancies, suggesting a stronger correlation with the decrease in O'' ratio as observed in the XPS results. For samples subjected to reduction, an increase in surface hydroxyl groups due to the introduction of OH in the process led to an observed increase in Ni³⁺ ratio. However, in contrast, the O'' ratio decreased, indicating a reduction in oxygen vacancies that exceeds the increase in hydroxyl groups. Moreover, at 700 °C, while the O'' ratio decreased significantly, the Ce³⁺ ratio did not decrease as significantly. This implies that the reduction in O'' is mostly due to a decrease in hydroxyl groups.

It was observed that XRD results showed the NiO peaks only in the oxidized samples, although the 700 °C sample showed weak NiO peak intensity due to the low Ni wt% (i.e., 3.9 wt%). In the case of the 400 °C and 500 °C treated samples, although Ni wt% was very similar (i.e., 9.9 and 9.4 wt%, respectively), 5.3 NiO_x/CeO₂-500Oxi sample's NiO peak intensity was much higher than that of 5.3 NiO_x/CeO₂-400Oxi sample's one. The results provide that formation of NiO is directly related to the calcination temperature. For reduced samples, 400 °C treated sample contained both NiO and metallic Ni peaks, indicating that 400 °C was not enough to transfer NiO to Ni under the current experimental conditions. In the case of the 500 °C and 700 °C reduced samples, Ni was dominant species, while 5.3 NiO_x/CeO₂-700R sample's intensity was weak due to relatively lower concentration of nickel particle. Although the XRD is a bulk technique, the results clearly provided the evidence of the oxidation state changing of surface NiO_x from Ni²⁺ to Ni⁰. In addition to the BET and Raman spectroscopy results, the XRD also provided that the crystallinity and crystallite size of CeO₂ were depended on the pretreatment temperature. For instance, the XRD peak intensity of CeO₂ increased and became sharpened with increasing pretreatment temperature due to the sintering or agglomeration of CeO₂ under high temperature (Table 4).

4.2 Pretreatment effect on catalytic activity

As discussed above, the pretreatment conditions (oxidation and reduction) led to change in molecular structures and textural properties for both support (i.e., CeO₂) and supported catalysts (i.e., NiO_x/CeO₂). From the catalytic activity results (Fig. 1 and 2), it was shown that the lower temperature (i.e., 400 °C and 500 °C) pretreated samples showed the better catalytic performance compared to the higher temperature pretreated one (i.e., 700 °C). When comparing Fig. 1 and 2, it was also observed that the oxidized samples showed slightly higher catalytic performance than that of the reduced samples. These results indicate that the catalytic performance of pretreated 5.3 NiO_x/CeO₂ catalysts were not only directly affected by the temperature, but also related to the gas composition for the pretreatment procedures. In the case of the N₂O and N₂ formation (or products' selectivity), the chemical reaction of N₂O formation and decomposition could be related: (1) $2\text{NO} + \text{CO} \rightarrow \text{N}_2\text{O} + \text{CO}_2$ ($\Delta H_r^0 = -381.45\text{ kJ}$), (2)

$\text{N}_2\text{O} + \text{CO} \rightarrow \text{N}_2 + \text{CO}_2$ ($\Delta H_r^0 = -365.05$ kJ).^{40,52} Based on thermodynamic values, the N_2O formation could be favourable step compared to the N_2O decomposition for the N_2 formation. Although non-catalytic reaction is different to the catalytic reaction, the thermodynamic values and products' formation is well matched to the current experimental results. (Fig. 1 (c) and (d), Fig. 2 (c) and (d)) It should be noted that N_2 and N_2O could be formed through different reaction pathways: $2\text{NO} \rightarrow \text{N}_2 + \text{O}_2$ ($\Delta H_r^0 = -180.5$ kJ), $2\text{NO} \rightarrow \text{N}_2\text{O} + 0.5\text{O}_2$ ($\Delta H_r^0 = -98.45$ kJ), $2\text{N}_2\text{O} \rightarrow 2\text{N}_2 + 2\text{O}_2$ ($\Delta H_r^0 = -164.1$ kJ). However, these reactions are thermodynamically unfavourable compared to

reported that adsorbed NO (or NOx) on $\text{Ce}_{0.67}\text{Sn}_{0.33}\text{O}_2$ produced the $\text{N}_2\text{O}/\text{N}_2$ mixture at lower temperature (~ 200 °C) and considerable N_2 production at higher temperature (250–400 °C). The authors hypothesized that oxygen vacancies and Ce^{3+} surfaces increase the NO dissociation and the CO adsorption, respectively, at higher temperature which increase the N_2 and CO_2 production.⁵⁴ X. Zhang et al. and Sugi et al. also observed the N_2O formation at lower temperature or early stage at fixed reaction temperature (i.e., 200 °C) over $\text{CuO}_x/\text{CeO}_2\text{-Fe}_2\text{O}_3$ and $\text{Fe}_2\text{O}_3/\text{SiC}$ catalysts, respectively. The authors suggested that at high temperatures the N_2O reduced to N_2 instead of displacing by NO.^{55,56}

The temperature of N_2O decomposition (or N_2 formation) was affected by the pre-treatment conditions, especially under the high temperature reducing conditions. The N_2O decomposition temperature over the 5.3 $\text{NiO}_x/\text{CeO}_2\text{-700R}$ catalyst was much higher than that of other samples. It is worthwhile to note that NO or CO conversion and N_2 selectivity of 5.3 $\text{NiO}_x/\text{CeO}_2\text{-700R}$ didn't reach 100% up to 500 °C (62% for NO conversion, 44% for CO conversion, and 37% for N_2 selectivity at 500 °C). It might be deduced that decreased catalytic activity can be influenced by combination of the relatively lower concentration of Ni species (1.4%), lower specific surface area (22 m^2/g), and lower concentration of oxygen vacancies ($0.49 \times 10^{21} \text{ cm}^{-3}$) compared to other samples even fixing at the same surface density (5.3 Ni/nm^2). Furthermore, it was reported that surface oxygen vacancies can promote dissociation N_2O .⁵⁷ With this respect, low oxygen vacancy concentration (low I_D/I_{F2g}) of reduced 5.3 $\text{Ni}/\text{CeO}_2\text{-700R}$ might interrupt the second step of reaction mechanism (N_2O dissociation by CO). The relationship between catalytic performance (T_{50} for NO conversion) and physical properties (Raman peak intensity (I_D/I_{F2g}), specific surface area, and CeO_2 crystallite size) of the catalysts were shown in Fig. 9. For both oxidized and reduced catalysts, T_{50} value was increased (decreasing catalytic performance) with decreasing defect ratio (I_D/I_{F2g}) and SSA as well as increasing CeO_2 crystallite size, indicating that the catalytic performance of catalysts was mainly

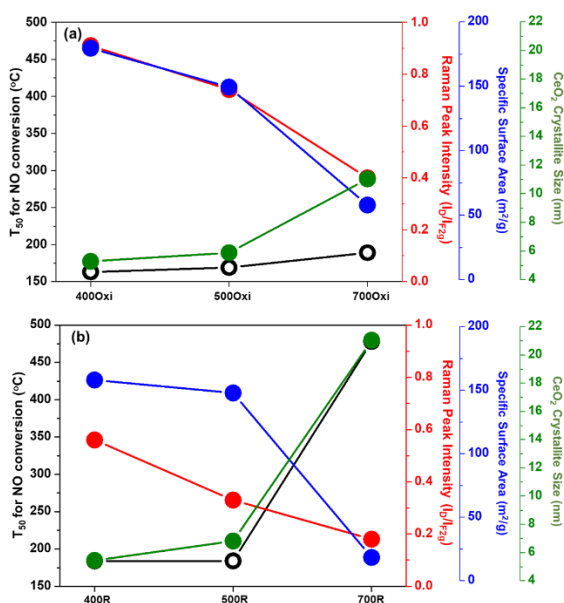


Fig. 9 Relationship between T_{50} for NO conversion and physical properties of (a) oxidized and (b) reduced 5.3 $\text{NiO}_x/\text{CeO}_2$ catalysts.

the two step mechanisms. Two step mechanisms over the diverse of catalysts (i.e., solid solution, supported catalysts) have been reported for NO reduction by CO. X. Yao et al.,

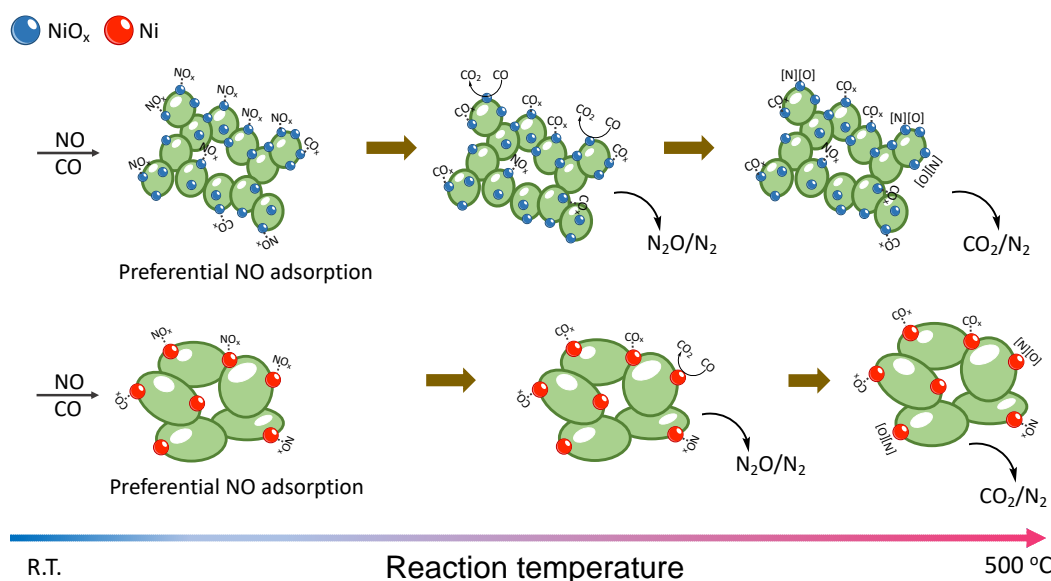


Fig. 10 Possible reaction mechanism for NO reduction by CO over (a) $\text{NiO}_x/\text{CeO}_2\text{-400xi}$ and (b) $\text{NiO}_x/\text{CeO}_2\text{-700R}$. The yellow spheres indicate NiO_x and the red spheres indicate Ni.

affected by the physicochemical properties (oxygen vacancies/defect sites, SSA, oxidation state of Ni) at fixed surface density of nickel (Ni atoms/nm²). The results based on reported literatures, which investigated NO reduction by CO reaction using various materials, supports, and synthesis methods, are summarized in Table S1 (based on T_{50} for the NO conversion ($T_{50,NO}$) and T_{50} for the CO conversion ($T_{50,CO}$)). $T_{50,NO}$ ranged from 102 °C to 498 °C, and $T_{50,CO}$ varied from 142 °C to 470 °C. The synthesis method also significantly influenced the activity, but from the perspective of materials, catalysts with CeO₂-based materials as the support showed lower T_{50} (Pd/CeZrO₂, $T_{50,NO}$ = 102 °C) and CuO as the active material generally achieved lower T_{50} (CuO/CeO₂, $T_{50,NO}$ = 125 °C). In contrast, catalysts using TiO₂ or Al₂O₃ as supports typically showed higher T_{50} (Pd/Al₂O₃, $T_{50,NO}$ = 279 °C, CuO/TiO₂, $T_{50,NO}$ = 290 °C). In this work, the prepared catalyst 5.3 NiO_x/CeO₂-400Oxi achieved relatively low $T_{50,NO}$ (167 °C) and $T_{50,CO}$ (175 °C).

4.3 Reaction mechanism of NO reduction by CO

Based on the physicochemical characterization results and *in-situ* DRIFTS, a possible reaction mechanism for NO reduction by CO could be proposed for both catalysts, 5.3 NiO_x/CeO₂-400Oxi and 5.3 NiO_x/CeO₂-700R (Fig. 10). Taking the 5.3 NiO_x/CeO₂-400Oxi catalyst as an example, at low temperatures, rather than CO, NO is mainly adsorbed in the several forms of nitrate or nitrite species owing to unpaired electron of NO. Then, as the temperature gradually increases up to 220 °C, adsorbed NO gradually undergoes desorption, decomposition, and transformation into N₂O and N₂. At the same time, a few amounts of CO is also adsorbed on the catalytic surface at low temperature, and as the temperature increases, CO adsorption becomes more significant. Adsorbed CO reduces the surface of the catalyst (Ce⁴⁺ → Ce³⁺) resulting in the formation of more surface oxygen vacancies. Increasing the presence of surface Ce³⁺ facilitates additional adsorption sites for CO_x species (CO and CO₂), which, in turn, weakens the N–O bond and enhances the dissociation of NO_x. According to widely accepted studies^{40,57}, surface Ce³⁺ plays a crucial role in facilitating the adsorption of CO species. Xiong et al. indicated that the dissociation of NO is a critical step in the NO+CO reaction, and the presence of oxygen vacancies weakens the N–O bonds, promoting their dissociation.⁵⁸ Additionally, Yao et al demonstrated that surface oxygen vacancies contribute significantly to the dissociation of N₂O.⁵⁴ Consequently, this promotes the formation of N₂ and CO₂ as the end products from 190 °C. It is expected that the reaction mechanism of 5.3 NiO_x/CeO₂-700R is similar to 5.3 NiO_x/CeO₂-400Oxi. However, the reaction is expected to occur at a higher temperature. This is likely attributed to differences in the catalyst's physicochemical properties, such as lower surface area and fewer oxygen vacancies in 5.3 NiO_x/CeO₂-700R compared to 5.3 NiO_x/CeO₂-400Oxi.

5. Conclusions

In this study, CeO₂ support materials were firstly pretreated under oxidation and reduction conditions at different temperatures (i.e., 400, 500, and 700 °C). The NiO_x supported

on the pretreated CeO₂ catalysts were synthesized at the same conditions that were used for CeO₂ support with a surface density of 5.3 Ni/nm². ICP/OES results confirmed that the Ni wt% and SD values were similar to the target values that were calculated by using synthesized sample's SSA. Afterwards, the NO reduction by CO reaction over synthesized catalysts were investigated to understand the relationship between catalyst synthesis conditions and the catalytic activity. From BET (Table 1) and XRD (Fig. 7) results, it was clearly shown that increased pretreatment temperature led to formation of NiO (oxidation) and metallic Ni species (reduction), decreased in SSA and increased in crystallite size of CeO₂ support. The Visible and UV Raman (Fig. 4 and 5) results provided that the concentration of oxygen vacancy and defect sites, which is crucial to enhance the catalytic activity, were decreased with increasing pretreatment temperature. The XPS results provided information about the oxidation state of the catalyst's surface, indicating the concentration of oxygen vacancies. Consistent with the Raman results, it was observed that as the pretreatment temperature increased, the concentration of oxygen vacancies decreased. Catalytic activity of both oxidized and reduced NiO_x/CeO₂ catalysts were decreased with increasing pretreatment temperature, while the oxidized catalysts showed slightly higher activity than those of reduced samples. From *in situ* DRIFTS results, NO-based surface species were mainly adsorbed on the active sites (Ni⁺ or Ni²⁺) at lower temperature (<250 °C), then were converted to N₂O species by means of exposing CO at 200–250 °C. After N₂O intermediate species formed, CO-based surface species occupied on the surface of active sites. Finally, N₂O could be further reduced to N₂ and formed Ni–NO (or Ni–CO) at higher temperature (> 200 °C). CO₂ produced through the carbonate species formation and decomposition on the catalyst surface that was pre-occupied by NO dominantly. Based on physicochemical and activity results, it can be concluded that catalytic activity of pretreated NiO_x/CeO₂ catalysts were mainly controlled by the physical properties of the catalysts.

Author Contributions

K. Lee: Methodology, Formal analysis, Writing – original draft, Writing – review & editing, B. Kim: Formal analysis, Writing – original draft, Writing – review & editing, J. Lee: Formal analysis, Writing – review & editing, G. Kwon: Formal analysis, Writing – review & editing, K. Yoon: Formal analysis, H. Song: Formal analysis, K. Min: Formal analysis, S. Shim: Funding acquisition, S. Hwang: Funding acquisition, T. Kim: Supervision, Writing – original draft, Writing – review & editing, Project administration, Funding acquisition. All authors have given approval to the final version of the manuscript.

Conflicts of interest

There are no conflicts of interest to declare.

Acknowledgements

The authors acknowledge funding support from the National Science Foundation (NSF-CBET-2050824). The authors would also like to thank the Advanced Energy Research and Technology Center (AERTC) for the facilities at the Stony Brook University. This research used the beamline 28-ID-1 of the National Synchrotron Light Source II (NSLS-II), which is U.S. Department of Energy (DOE) Office of Science User Facilities at Brookhaven National Laboratory under Contract No. DE-SC0012704. This research was supported by the MOTIE (Ministry of Trade, Industry, and Energy) in Korea, under the Human Resource Development Program for Industrial Innovation (Global) (P0017303, Smart Manufacturing Global Talent Training Program) supervised by the Korea Institute for Advancement of Technology (KIAT).

References

- 1 G. Zhiming, D. Qianzi, M. Hongwei and L. Zhanping, *Journal of Rare Earths*, 2016, 34, 1213–1220.
- 2 E. D. Arabaci, A. M. Önal and S. Özkar, *Journal of The Electrochemical Society*, 2020, 167, 106513.
- 3 L. He, B. Liang, L. Li, X. Yang, Y. Huang, A. Wang, X. Wang and T. Zhang, *Acs Catalysis*, 2015, 5, 1623–1628.
- 4 W. Zou, C. Ge, M. Lu, S. Wu, Y. Wang, J. Sun, Y. Pu, C. Tang, F. Gao and L. Dong, *RSC advances*, 2015, 5, 98335–98343.
- 5 Z. Liu, S. Yao, A. Johnston-Peck, W. Xu, J. A. Rodriguez and S. D. Senanayake, *Catalysis Today*, 2018, 311, 74–80.
- 6 X. Du, D. Zhang, L. Shi, R. Gao and J. Zhang, *The Journal of Physical Chemistry C*, 2012, 116, 10009–10016.
- 7 Y. Wang, A. Zhu, Y. Zhang, C. Au, X. Yang and C. Shi, *Applied Catalysis B: Environmental*, 2008, 81, 141–149.
- 8 X. Cheng, A. Zhu, Y. Zhang, Y. Wang, C. Au and C. Shi, *Applied Catalysis B: Environmental*, 2009, 90, 395–404.
- 9 C. Tang, B. Sun, J. Sun, X. Hong, Y. Deng, F. Gao and L. Dong, *Catalysis Today*, 2017, 281, 575–582.
- 10 S. Zhang, J. Lee, D. H. Kim and T. Kim, *Catalysis Science & Technology*, 2020, 10, 2359–2368.
- 11 K.-M. Lee, G. Kwon, S. Hwang, J. A. Boscoboinik and T. Kim, *Catalysis Science & Technology*, 2021, 11, 7850–7865.
- 12 R. L. Martins and M. Schmal, *Journal of the Brazilian Chemical Society*, 2014, 25, 2399–2408.
- 13 E. Mamontov, T. Egami, R. Brezny, M. Koranne and S. Tyagi, *The Journal of Physical Chemistry B*, 2000, 104, 11110–11116.
- 14 P. Snytnikov, M. Popova, Y. Men, E. Rebrov, G. Kolb, V. Hessel, J. Schouten and V. Sobyannin, *Applied Catalysis A: General*, 2008, 350, 53–62.
- 15 S. Zhang, Y. Li, J. Huang, J. Lee, D. H. Kim, A. I. Frenkel and T. Kim, *The Journal of Physical Chemistry C*, 2019, 123, 7166–7177.
- 16 I. Iglesias, A. Quindimil, F. Marino, U. De-La-Torre and J. R. González-Velasco, *international journal of hydrogen energy*, 2019, 44, 1710–1719.
- 17 C. A. Roberts, D. Prieto-Centurion, Y. Nagai, Y. F. Nishimura, R. D. Desautels, J. Van Lierop, P. T. Fanson and J. M. Notestein, *The Journal of Physical Chemistry C*, 2015, 119, 4224–4234.
- 18 T. C. Peck, G. K. Reddy, M. Jones and C. A. Roberts, *The Journal of Physical Chemistry C*, 2017, 121, 8435–8443.
- 19 T. C. Peck, G. K. Reddy and C. A. Roberts, *Catalysis Science & Technology*, 2019, 9, 1132–1140.
- 20 T. Kim, A. Burrows, C. J. Kiely and I. E. Wachs, *Journal of Catalysis*, 2007, 246, 370–381.
- 21 S. Vivek, S. Preethi, T. V. Kumar, A. K. Sundramoorthy and K. S. Babu, *Journal of Alloys and Compounds*, 2020, 816, 152608.
- 22 C. Wu, Z. Xiao, L. Wang, G. Li, X. Zhang and L. Wang, *Catalysis Science & Technology*, 2021, 11, 1965–1973.
- 23 S. D. Senanayake, J. Evans, S. Agnoli, L. Barrio, T.-L. Chen, J. Hrbek and J. A. Rodriguez, *Topics in Catalysis*, 2011, 54, 34–41.
- 24 J. Carrasco, L. Barrio, P. Liu, J. A. Rodriguez and M. V. Ganduglia-Pirovano, *The Journal of Physical Chemistry C*, 2013, 117, 8241–8250.
- 25 T. Xu, J. Xue, X. Zhang, G. He and H. Chen, *Applied Surface Science*, 2017, 402, 294–300.
- 26 J. Taghavimoghaddam, G. P. Knowles and A. L. Chaffee, *Journal of Molecular Catalysis A: Chemical*, 2012, 358, 79–88.
- 27 M. Daniel and S. Loidant, *Journal of Raman Spectroscopy*, 2012, 43, 1312–1319.
- 28 I. Kosacki, T. Suzuki, H. U. Anderson and P. Colomban, *Solid State Ionics*, 2002, 149, 99–105.
- 29 J. E. Spanier, R. D. Robinson, F. Zhang, S.-W. Chan and I. P. Herman, *Physical Review B*, 2001, 64, 245407.
- 30 W. Weber, K. Hass and J. McBride, *Physical Review B*, 1993, 48, 178.
- 31 T. Taniguchi, T. Watanabe, N. Sugiyama, A. Subramani, H. Wagata, N. Matsushita and M. Yoshimura, *The Journal of Physical Chemistry C*, 2009, 113, 19789–19793.
- 32 M.-F. Luo, Z.-L. Yan, L.-Y. Jin and M. He, *The Journal of Physical Chemistry B*, 2006, 110, 13068–13071.
- 33 Z. Wu, M. Li, J. Howe, H. M. Meyer III and S. H. Overbury, *Langmuir*, 2010, 26, 16595–16606.
- 34 T. Livneh and E. Sterer, *Physical Review B*, 2006, 73, 085118.
- 35 K.-M. Lee, M. Brito, J. DeCoster, K. Linskens, K. Mehdi, W.-I. Lee, E. Kim, H. Kim, G. Kwon, C.-Y. Nam, and T. Kim, *Molecular Catalysis*, 2022, 528, 112465.
- 36 C. Deng, Q. Huang, X. Zhu, Q. Hu, W. Su, J. Qian, L. Dong, B. Li, M. Fan and C. Liang, *Applied Surface Science*, 2016, 389, 1033–1049.
- 37 L. Atzori, M. G. Cutrufello, D. Meloni, B. Onida, D. Gazzoli, A. Ardu, R. Monaci, M. F. Sini and E. Rombi, *Frontiers of Chemical Science and Engineering*, 2021, 15, 251–268.
- 38 N. Jayababu, M. Poloju, J. Shruthi and M. R. Reddy, *RSC advances*, 2019, 9, 13765–13775.
- 39 L. Liu, B. Liu, L. Dong, J. Zhu, H. Wan, K. Sun, B. Zhao, H. Zhu, L. Dong and Y. Chen, *Applied Catalysis B: Environmental*, 2009, 90, 578–586.
- 40 C. Deng, M. Li, J. Qian, Q. Hu, M. Huang, Q. Lin, Y. Ruan, L. Dong, B. Li and M. Fan, *Chemistry—An Asian Journal*, 2016, 11, 2144–2156.

- 41 X. Zhang, H. He, H. Gao and Y. Yu, *Spectrochimica Acta Part A: Molecular and Biomolecular Spectroscopy*, 2008, 71, 1446–1451.
- 42 X. Dai, W. Jiang, W. Wang, X. Weng, Y. Shang, Y. Xue and Z. Wu, *Chinese Journal of Catalysis*, 2018, 39, 728–735.
- 43 N. Liu, X. Chen, J. Zhang and J. W. Schwank, *Catalysis Today*, 2015, 258, 139–147.
- 44 L. Zhang, X. Yao, Y. Lu, C. Sun, C. Tang, F. Gao and L. Dong, *Journal of colloid and interface science*, 2018, 509, 334–345.
- 45 S. Gaur, H. Wu, G. G. Stanley, K. More, C. S. Kumar and J. J. Spivey, *Catalysis today*, 2013, 208, 72–81.
- 46 X. Cheng, Y. Cheng, Z. Wang and C. Ma, *Fuel*, 2018, 214, 230–241.
- 47 M. Mihaylov, K. Chakarova and K. Hadjiivanov, *Journal of Catalysis*, 2004, 228, 273–281.
- 48 Z. Wang, F. Lin, S. Jiang, K. Qiu, M. Kuang, R. Whiddon and K. Cen, *Fuel*, 2016, 166, 352–360.
- 49 C. Yang, Y. Lu, L. Zhang, Z. Kong, T. Yang, L. Tao, Y. Zou and S. Wang, *Small Structures*, 2021, 2, 2100058.
- 50 T. Hattori, K. Kobayashi and M. Ozawa, *Japanese Journal of Applied Physics*, 2016, 56, 01AE06.
- 51 A. P. Grosvenor, M. C. Biesinger, R. S. C. Smart and N. S. McIntyre, *Surface Science*, 2006, 600, 1771–1779.
- 52 D. Prieur, W. Bonani, K. Popa, O. Walter, K. W. Kriegsman, M. H. Engelhard, X. Guo, R. Eloirdi, T. Gouder and A. Beck, *Inorganic Chemistry*, 2020, 59, 5760–5767.
- 53 L. Xue, C. Zhang, H. He and Y. Teraoka, *Applied Catalysis B: Environmental*, 2007, 75, 167–174.
- 54 X. Yao, C. Tang, Z. Ji, Y. Dai, Y. Cao, F. Gao, L. Dong and Y. Chen, *Catalysis Science & Technology*, 2013, 3, 688–698.
- 55 X. Zhang, X. Cheng, C. Ma and Z. Wang, *Catalysis Science & Technology*, 2018, 8, 3336–3345.
- 56 Y. Sugi, N. Todo and T. Sato, *Bulletin of the Chemical Society of Japan*, 1975, 48, 337–338.
- 57 X. Yao, Q. Yu, Z. Ji, Y. Lv, Y. Cao, C. Tang, F. Gao, L. Dong and Y. Chen, *Applied Catalysis B: Environmental*, 2013, 130, 293–304.
- 58 Y. Xiong, X. Yao, C. Tang, L. Zhang, Y. Cao, Y. Deng, F. Gao and L. Dong, *Catalysis Science & Technology*, 2014, 4, 4416–4425.